

1 Lowering of glacial $p\text{CO}_2$ in response to changes in
2 oceanic circulation and marine biogeochemistry

3

4

5 Victor Brovkin^{*1}, Andrey Ganopolski¹, David Archer², Stefan Rahmstorf¹

6

7 ¹Potsdam Institute for Climate Impact Research, P.O.Box 601203, Potsdam, Germany

8 ²Department of Geophysical Sciences, University of Chicago, 5734 S Ellis Ave,
9 Chicago, Ill 60637, U.S.A.

10

11

12 *corresponding author, Tel. +49(0)3312882592, fax +49(0)3312882570, e-mail:
13 victor@pik-potsdam.de

Submitted to Paleoceanography
19 October 2006

1 **Abstract**

2 We use a model of intermediate complexity, CLIMBER-2, to investigate what recent
3 improvements in the representation of the physics and biology of the glacial ocean
4 imply for the atmospheric CO₂ concentration. The coupled atmosphere-ocean model is
5 able to reproduce the deep, salty, stagnant water mass inferred from Antarctic deep
6 pore-water data [Adkins *et al.*, 2002] and the changing temperature of the entire deep
7 ocean [Martin *et al.*, 2002]. When the pH feedback of the sedimentary CaCO₃ cycle is
8 included in the model, we find a drawdown of 43 ppm resulting from this physical
9 circulation change. Fertilizing the Atlantic and Indian sectors of the Southern Ocean
10 north of the polar front leads to a further drawdown of 37 ppm. Other changes to the
11 glacial carbon cycle include a decrease in the amount of carbon stored in the terrestrial
12 biosphere (540 GtC), which increases *p*CO₂ by 15 ppm, and a change in ocean salinity
13 resulting from a drop in sea level, which increases *p*CO₂ by another 12 ppm. A decrease
14 in shallow water CaCO₃ deposition draws down *p*CO₂ by 12 ppm. In total, the model is
15 able to explain more than two thirds (65 ppm) of the glacial to interglacial *p*CO₂ change,
16 based only on mechanisms that are clearly documented in the proxy data. A good match
17 between simulated and reconstructed distribution of δ¹³C changes in the deep Atlantic
18 [Duplessy *et al.*, 1988] suggests that the model captures the mechanisms of
19 reorganization of biogeochemistry in the Atlantic ocean reasonably well. Additional,
20 poorly documented potential mechanisms to explain the rest of the observed drawdown
21 include changes in the organic carbon:CaCO₃ ratio of sediment rain reaching the sea
22 floor, iron fertilization in the sub-Antarctic Pacific ocean, and changes in terrestrial
23 weathering.

1 **Introduction**

2 More than two decades after their discovery, the cause of the glacial pCO₂ cycles
3 remains a scientific challenge [*Broecker and Peng*, 1982; *Archer et al.*, 2000; *Sigman*
4 *and Boyle*, 2000]. The rise and fall of atmospheric CO₂ levels is an integral part of the
5 glacial cycles, accounting for 30-35% of the temperature changes over the glacial cycle
6 [*Schneider von Deimling et al.*, 2006b]. Our inability to hindcast or even explain the
7 CO₂ variations of the past undermines our ability to predict the future response of the
8 carbon cycle and climate to anthropogenic carbon emissions [*Scheffer et al.*, 2006; *Torn*
9 *and Harte*, 2006].

10 Ice-core records show a remarkable correlation between atmospheric CO₂ and
11 Antarctic temperature. This correlation was evident in the original Vostok record to 400
12 kyr [*Petit et al.*, 1999] and has recently been extended to 650 kyr [*Siegenthaler et al.*,
13 2005]. Paleoclimate records rarely correlate with this degree of reliability and
14 simplicity, spurring a search for a single dominant mechanism, based on or related to
15 the temperature of Antarctica, to explain the glacial CO₂ cycles.

16 CO₂ solubility in seawater increases with decreasing temperature, and the temperature
17 of the deep sea is an obvious place to look. Deep ocean temperature may be related to
18 temperatures in Antarctica by the outcropping of the abyssal water mass in the high
19 Southern latitudes. Paleo-temperature records of the deep Pacific ocean based on Mg/Ca
20 ratios of foraminifera show temperature changes of 2-4°C over glacial cycles [*Martin et*
21 *al.*, 2002]. Abyssal temperatures have also been reconstructed from pore-water δ¹⁸O
22 data by *Adkins et al.* [2002], likewise showing a glacial-interglacial temperature range
23 of 2 to 4°C. If ocean temperature were a dominant control on atmospheric CO₂, this
24 would result in a positive feedback between temperature and CO₂ that would amplify
25 any initial temperature change forced by orbital changes [*Archer et al.*, 2004]. This
26 feedback could also ultimately amplify CO₂ concentration changes from fossil fuel
27 combustion [*Scheffer et al.*, 2006; *Torn and Harte*, 2006].

28 A single core from the Southern Ocean in the *Adkins et al.* [2002] dataset revealed an
29 abyssal water mass of extremely high salinity, higher than the increase in ocean mean
30 salinity that resulted from the lowering of sea level. Subsequent reconstruction of the

1 ^{14}C content of deep water through time, from analysis of benthic corals, shows that this
2 deep salty water mass was extremely isolated from the atmosphere.

3 Some coupled climate models of the glacial ocean circulation are able to reproduce
4 this stagnant salty water mass, by altering the fresh water balance of the Southern Ocean
5 [Schmittner, 2003; Shin *et al.*, 2003]. With the colder glacial climate, sea ice is able to
6 survive the trip north to cross the latitude of the polar front. Fresh water carried by the
7 ice leaves behind a polar convection region of higher salinity. This mechanism has been
8 included in recent box model studies [Kohler *et al.*, 2005; Watson and Garabato, 2006]
9 and a study using an oceanic general circulation model [Toggweiler *et al.*, 2006]. With
10 our model, we are able to simulate explicitly changes in atmospheric and oceanic
11 circulations in response to glacial changes in radiative forcing. Our results in this paper
12 represent the first quantitative assessment of the impact of interactive circulation
13 structure on the $p\text{CO}_2$ of the atmosphere, in particular the deep salt stratification in the
14 Southern Ocean [Adkins *et al.*, 2002], including the effects of the sediment CaCO_3
15 feedback to $p\text{CO}_2$, via changes in ocean pH.

16 Another recent publication by Kohfeld *et al.* [2005] explored evidence for enhanced
17 glacial marine productivity, i.e. the "biological pump", another potential mechanism of
18 lowering glacial $p\text{CO}_2$. They found that proxy data support increased marine production
19 during LGM in the Atlantic and Indian sectors of the sub-Antarctic ocean, north of the
20 Antarctic polar front. South of the front, the proxy data indicate decreased productivity.
21 Data from the Pacific sector of the Southern Ocean are sparse and equivocal. An
22 enhancement of global oceanic marine productivity during the LGM is supported by
23 model studies [Bopp *et al.*, 2003].

24 We will show our finding that neither of these mechanisms is sufficient to explain the
25 entire magnitude of the atmospheric CO_2 changes between glacial and interglacial
26 times. The high correlation between $p\text{CO}_2$ and temperature spurs a search for a single
27 mechanism, but we are forced to consider the possibility that glacial $p\text{CO}_2$ changes are
28 driven not by a single mechanism but a combination of different factors. This strategy is
29 also necessitated by the existence of changes in the carbon cycle in which we are fairly
30 confident, such as changes in shallow-water CaCO_3 deposition, or the amount of carbon
31 stored in the terrestrial biosphere. In the absence of a single plausible explanation for
32 the CO_2 cycles, we search for a "CO₂ stew" of mechanisms which, combined, can

1 account for the entire CO₂ change, without violation of proxy paleoceanographic
2 constraints on the glacial carbon cycle.

3 **Methods**

4 Our investigation is based on an Earth system model of intermediate complexity,
5 CLIMBER-2, that is fast enough to carry out simulations on a scale of ten thousand
6 years while its geographical explicitness allows accounting for spatial changes in
7 atmospheric, oceanic, and biogeochemical dynamics. The CLIMBER-2 model includes
8 a statistical-dynamical atmospheric model with 10°x51° resolution, a zonally-averaged
9 3-basin dynamic oceanic model with 2.5° zonal resolution, a sea ice model, a terrestrial
10 biosphere model, an oceanic biogeochemistry model, and a phosphate-limited model for
11 marine biota [Petoukhov *et al.*, 2000; Ganopolski *et al.*, 2001; Brovkin *et al.*, 2002a].

12 Carbonate compensation is simulated by a model of deep sea sediment diagenesis
13 [Archer, 1991] coupled to CLIMBER-2. The sediment model operates on the
14 CLIMBER-2 spatial resolution with one extension: While the ocean circulation model
15 has vertical basin boundaries, the sediment model accounts for realistic oceanic
16 hypsometry by calculating the fractional area of the grid cell floor at every intermediate
17 model depth (14 layers from 500 to 5000 m). In polar regions, deep-sea sedimentation
18 of carbonates does not occur. This is captured in the model by a reduction in CaCO₃
19 sedimentation by a factor f which is a semi-empirical function of sea surface
20 temperature, T_s :

$$21 \quad f = \frac{e^{T_s - T_0}}{5 + e^{T_s - T_0}}, \quad (1)$$

22 where T_0 is equal to 3.5°C.

23 The flux of dust to the sea floor, r_{clay} , is estimated by a correlation with organic
24 production, r_{org} , based on the present-day detrital rain rate to the sea floor:

$$25 \quad r_{clay} = 1.8 \cdot 10^{-5} \cdot (r_{org})^{1.41}. \quad (2)$$

26 The production ratio of CaCO₃ to organic carbon in the surface ocean is fixed to 0.12.
27 This model parameter is tuned to best reproduce observed DIC and alkalinity fields in
28 the pre-industrial simulation CTRL.

1 A list of simulations is shown in Table 1. We performed five glacial simulations with
2 five factors added consecutively, one factor after another. We started from a glacial
3 climate simulation (G), then added enhanced nutrient utilization in the subpolar
4 Southern Ocean (GN), land carbon release (GNL), sea level change (GNLS), and
5 shallow water carbonate sedimentation (GNLSC). Details of these simulations are
6 explained in the Results section below.

7 In all glacial simulations G to GNLSC, the radiative effect of the CO₂ concentration
8 was imposed (constant) in order to exclude the complicating effect of the climate to CO₂
9 feedback. The atmospheric CO₂ concentration was set to 180 ppm which roughly
10 accounts for the effect of glacial CH₄ and N₂O lowering assuming a typical LGM CO₂
11 concentration of 200 ppm. The radiative effect of the elevated dust concentration in the
12 glacial atmosphere was not accounted for (according to simulations by *Schneider von*
13 *Deimling et al.* [2006b], this forcing could lead to an additional 1°C global cooling).
14 The distribution of ice sheets was prescribed following *Peltier* [1994], and orbital
15 forcing was taken as of 21,000 yr BP [*Berger*, 1978]. Silicate weathering, volcanic CO₂
16 outgassing, and organic carbon weathering and burial were neglected. The CaCO₃ cycle
17 included CaCO₃ weathering at a prescribed rate (equal to the deep-sea burial of CaCO₃
18 in the present-day control run CTRL), and deep sea burial of CaCO₃, predicted by the
19 sediment model. The sedimentary feedback to ocean pH, calcium carbonate
20 compensation, was active in all glacial simulations. Dust deposition input to the
21 sediment model for glacial time was doubled from the control simulation to account for
22 increased dust load during the LGM [*Rea*, 1994; *Mahowald et al.*, 1999]. All
23 simulations were integrated for 50,000 years to allow the weathering and sedimentary
24 CaCO₃ cycle to approach equilibrium.

25 **Results**

26 **Simulated glacial climate**

27 The climate model under a complete set of glacial forcings (except dust, sea above)
28 simulates a global surface air temperature cooling by 5°C, and globally averaged SST
29 and volume averaged ocean temperature decreased by 3°C. The main changes in
30 oceanic circulation are associated with a weakening (by ca. 30%) and shoaling of the
31 Atlantic meridional overturning cell and intensification of AABW formation, with a

1 much stronger penetration of AABW into the Atlantic Ocean. While in the present-day
2 CTRL simulation AABW is present only in the Southern Atlantic (Fig. 1a), in the
3 glacial simulations AABW fills the whole Atlantic basin below 2,500 meters (Fig. 1b).

4 Enhanced AABW formation is primarily caused by more extensive sea ice formation
5 and an associated brine rejection around Antarctica. The simulated annual area of sea
6 ice under LGM condition is twice larger than at present. This large sea ice expansion
7 leads to an increase of the sea ice transport out of the area of AABW formation, which
8 increases salinity of AABW by 0.5 psu (in addition to the 1 psu of global increase of
9 salinity due to sea level drop) and decreases surface salinity in the Atlantic Ocean (Fig.
10 1b). The simulated increase of AABW salinity is consistent although somewhat smaller
11 than the deep pore-water estimates by *Adkins et al.* [2002]. Although NADW cools
12 more than AABW under the glacial conditions, the relative increase of AABW salinity
13 and a relative decrease of NADW salinity overwhelms the temperature effect and the
14 density of glacial AABW becomes higher than the density of NADW. This allows
15 AABW to occupy a much larger portion of the deep Atlantic, and causes a shoaling and
16 a weakening of the Atlantic meridional circulation. In the Pacific, there is little change
17 in the circulation field, but changes in temperature are comparable to the Atlantic and
18 similar to reconstructions by *Martin et al.* [2002] (Fig. 2a).

19 **Modeled glacial biogeochemistry**

20 Simulation G: effect of changes in circulation and sea surface temperatures

21 The full drawdown of atmospheric pCO₂, after amplification by the CaCO₃ cycle, is
22 43 ppm (Table 2). The average temperature change of the ocean was 3°C, so the CO₂
23 drawdown amounts to 12 ppm/°C. This is higher than the 8-10 ppm/°C estimate from a
24 set of solubility experiments using the POP GCM [*Martin et al.*, 2005], in part because
25 of the increase in volume of the high-carbon AABW water mass which was not
26 accounted for in that model. The maximum increase in the DIC concentration, 100
27 μmol/kg, is found in the deep North Atlantic, where the boundary between AABW and
28 NADW has changed. The CO₂ drawdown is also enhanced by the effect of the CaCO₃
29 cycle. Acidification of deep waters leads to a temporary reduction in carbonate sediment
30 preservation until a balance between weathering and sedimentation is achieved. This

1 process of carbonate compensation results in increased total oceanic alkalinity which
2 decreases atmospheric $p\text{CO}_2$ level further.

3 Temporal dynamics of atmospheric $p\text{CO}_2$ in the G simulation (Fig. 3) demonstrates
4 several stages of the model response to the imposed glacial boundary conditions. During
5 the first 500 years, $p\text{CO}_2$ level drops by 18 ppm in response to the surface ocean
6 cooling. The $p\text{CO}_2$ drawdown by additional 15 ppm during the next 2,000 years is a
7 response to the reorganization of the oceanic circulation. A further slow decrease by 10
8 ppm is associated with carbonate compensation.

9

10 Simulation GN: G plus iron fertilization

11 In the GN simulation, the biological pump in the Atlantic and Indian sectors of the
12 sub-Antarctic ocean (30 to 50°S) was stimulated to complete drawdown of nutrient
13 (PO_4) in the surface ocean imitating a productivity increase during LGM in these
14 regions detected by *Kohfeld et al.* [2005], probably the result of iron fertilization from
15 Patagonian dust [*Mahowald et al.*, 1999]. The globally-averaged export flux at the
16 surface increased by 1.8 PgC/yr (about 20% of CTRL level) and atmospheric CO_2
17 dropped by 37 ppm in comparison with the G simulation (Table 2). This value is higher
18 than the 15-ppm effect found by *Bopp et al.* [2003] in an ocean-biogeochemistry model
19 run driven by the LGM dust flux, but that study did not include the effect of carbonate
20 compensation. In comparison with the G simulation, the DIC concentration mainly
21 increased in Southern Ocean and deep ocean (Fig. 4a). This increase is pronounced not
22 only in the Atlantic and Indian oceans where the forcing was applied, but also in the
23 Pacific Ocean, which is linked to the Atlantic and Indian through the Southern Ocean.

24 Simulations GNL and GNLS: GN plus land carbon and sea level change

25 While the GN simulation explains almost the complete magnitude of glacial $p\text{CO}_2$
26 changes, we should not neglect several other factors that worked in the opposite
27 direction. Terrestrial pollen records reveal that during the LGM, forest cover was
28 strongly reduced: boreal forests were diminished due to ice sheet expansion and
29 increased aridity of continental interiors, while tropical forests had a more open canopy

1 due to increased aridity [Crowley, 1995; Prentice and Jolly, 2000]. Reduced
2 atmospheric CO₂ levels should have a direct negative effect on the plant productivity
3 through reduced water use efficiency [Harrison and Prentice, 2003]. Much of the land
4 surface in the high northern latitudes was covered by ice sheets, although this reduction
5 in forested area was partly compensated for by exposed tropical shelf areas in South-
6 East Asia, likely populated by forest.

7 The glacial reduction in forest cover simulated by the CLIMBER-2 model leads to a
8 cooling of about 1°C due to increased surface albedo and reduced transpiration [Jahn *et*
9 *al.*, 2005]. These biogeophysical effects are accounted in the glacial simulations
10 reported here. Model studies that account for climate, CO₂, and sea level changes during
11 the LGM suggest a net reduction of terrestrial carbon storage by 300 to 700 GtC
12 [Crowley, 1995; Francois *et al.*, 1999; Joos *et al.*, 2004]. Independently, glacial changes
13 in deep ocean δ¹³C have been interpreted as a reduction in land carbon storage by about
14 500 GtC. The interactive terrestrial biosphere model in CLIMBER-2 simulates a net
15 reduction in terrestrial carbon storage by 540 PgC. Accounting for this land carbon
16 release in the GNL simulation results in a *p*CO₂ increase by 15 ppm after carbonate
17 compensation (Table 2).

18 The buildup of ice sheets during glacial time led to reduced sea level that reached its
19 lowest point during the LGM. In the GNLS simulation, we assumed that a 3% decrease
20 in total ocean volume was accompanied by a 3% increase in total salinity, alkalinity,
21 and PO₄ concentrations. In response to these changes, atmospheric *p*CO₂ increased by
22 12 ppm.

23 Together, these land carbon and sea level effects lead to an increase in atmospheric
24 *p*CO₂ by 27 ppm. The oceanic DIC concentration is considerably increased (by about
25 150 μmol/kg) in comparison with the GN simulation (Fig. 4). This is mostly a sign of
26 dissolved land carbon, with a further contribution from the drop in sea level, amplified
27 by the carbonate compensation process (Table 2).

28 Simulation GNLSC: GNLS plus reduction in shallow water sedimentation

29 During the glacial period, coral reef area in tropical and subtropical shelf regions was
30 greatly reduced. Simulations of the ReefHab model by Kleypas [1997] suggested an

1 almost 4-fold reduction in coral reef production during the LGM. Our more mild
2 assumption here is that carbonate sedimentation in shallow waters was reduced by 50%
3 during the glacial time and that this sedimentation is approximately equal to deep-sea
4 carbonate sedimentation at present. Consequently, we imitated a decrease in shallow
5 water sedimentation by increasing weathering flux by 50% in the GNLSC simulation.
6 This results in further enhancement of the DIC and alkalinity concentrations and a
7 consequent $p\text{CO}_2$ drop by 12 ppm (Fig. 4c, Table 2). In the steady state, ocean
8 carbonate ion increases make the deep ocean more basic, until deep ocean CaCO_3 burial
9 balances the weathering flux. Ultimately, this scenario leads to an increase in deep sea
10 carbonate ion concentration and a deepening of the lysocline or carbonate compensation
11 depth (CCD).

12 Figure 5 presents a comparison of the fraction of CaCO_3 (%) in the upper sediment
13 layer. While a comparison of present-day observations averaged to the CLIMBER-2
14 grid (Fig. 5a) with model results in the CTRL simulation (Fig. 5b) shows clearly that the
15 model performance is far from perfect, it is able to capture several important features of
16 the carbonate distribution on the ocean floor. Firstly, the present-day CCD is located
17 deeper in the North Atlantic than in the South Atlantic, and this is reproduced by the
18 model. Secondly, the difference between Atlantic and Pacific basins is captured quite
19 well, as the CCD in the Pacific is shallower than in the Atlantic.

20 The CCD depth is not substantially changed in the simulation GNLS (Fig. 5c)
21 relatively to the CTRL simulation (Fig. 5c). This is expected because carbonate
22 compensation restores the deep-sea carbonate ion concentration to something close to
23 the CTRL value. In the GNLSC simulation the CCD deepens by about 500 meters,
24 resulting in a sedimentation shift to the model ocean floor of 5,000m in Southern ocean
25 (Fig. 5d). This is, perhaps, a stronger shift than would be supported by the glacial CCD
26 reconstruction [Catubig *et al.*, 1998].

27 Other mechanisms – changes in rain ratio, weavering, nutrients utilization in Pacific

28 Another mechanism that may have contributed to the lower glacial $p\text{CO}_2$ is a decrease
29 in carbonate to organic flux ratio [Archer and Maier-Reimer, 1994]. This mechanism
30 involves a shift from calcite- to silicate-producing plankton during glacial periods, for
31 example via the silica leakage mechanism [Matsumoto *et al.*, 2002]. CLIMBER-2 does

1 not simulate phytoplankton structure, but we tested the mechanism by reducing the rain
2 ratio from 0.12 to 0.1 in simulation GN. The ocean carbonate burial rate initially
3 decreases, driving the ocean toward the basic. The change in the equilibrium ocean
4 chemistry reduces $p\text{CO}_2$ by an additional 15 ppm (Table 3).

5 During the glacial maximum, river runoff was different from the Holocene because of
6 the large area covered with ice sheets, exposed shelf areas, and drier climate. Glacial
7 changes in terrestrial weavering (even direction of these changes) are uncertain, but they
8 were unlikely to be high [Munhoven, 2002]. We investigated a scenario of a 10%
9 reduction in the terrestrial weavering flux and found a $p\text{CO}_2$ increase by 2 ppmv in
10 response to these changes (Table 3).

11 *Kohfeld et al.* [2005] did not detect large glacial changes in the nutrient utilization in
12 Pacific sub-Antarctic, but this region is poorly populated with data. We performed an
13 additional model simulation with complete nutrient utilization in this region. The $p\text{CO}_2$
14 drawdown is 7 ppm, much less than 37 ppm in case of the Atlantic and Indian sub-
15 Antarctic (Table 3). This could be explained by the very small changes in glacial Pacific
16 circulation as compared to the glacial circulation changes in the Atlantic. Additionally,
17 surface nutrients concentration in Pacific sub-Antarctic was already drawn down by
18 complete utilization of surface nutrients in the Atlantic and Indian sectors of sub-
19 Antarctic.

20 Redistribution of $\delta^{13}\text{C}$

21 The distribution of $\delta^{13}\text{C}$ in the ocean is driven by several factors simultaneously:
22 changes in ocean circulation, biological pump, and land carbon storage. In Atlantic, a
23 change in the water mass distribution in the G simulation results in a decrease in $\delta^{13}\text{C}$
24 below 2000 m, with a maximum decrease in the deep North Atlantic, while $\delta^{13}\text{C}$ in the
25 upper ocean increases (Fig. 6a). The sub-Antarctic biological pump enhancement in the
26 GN simulation leads to a further increase in the $\delta^{13}\text{C}$ gradient between upper and deeper
27 waters (Fig. 6b), and a stronger decrease in $\delta^{13}\text{C}$ in the Antarctic ocean. These changes
28 are qualitatively in line with reconstructions of $\delta^{13}\text{C}$ distribution in the Atlantic by
29 *Duplessy et al.* [1988] and more recent synthesis of glacial $\delta^{13}\text{C}$ changes [Curry and
30 *Oppo*, 2005; *Toggweiler et al.*, 2006]. Release of terrestrial carbon in the GNLS

1 simulation causes an average $\delta^{13}\text{C}$ change in the ocean of -0.4‰ (Fig. 6c), a bit more
2 than the usual estimate of -0.35‰ [Shackleton, 1977].

3 When compared with the reconstruction of $\delta^{13}\text{C}$ changes by Duplessy *et al.* [1988],
4 quantitative changes in $\delta^{13}\text{C}$ in the North Atlantic are reproduced quite well by the
5 model (Fig. 7). Shallowing of NADW in our simulation is not as substantial as in the
6 reconstruction. The same is true for the deep Southern Ocean, where data suggest much
7 stronger changes in $\delta^{13}\text{C}$. In the Indian and Pacific basins, $\delta^{13}\text{C}$ increases above 2000 m
8 depth while these stages in $\delta^{13}\text{C}$ are reflected in the Figure 5.

9 Ice-core measurements of atmospheric $\delta^{13}\text{CO}_2$ during LGM [Smith *et al.*, 1999]
10 reveal little change between LGM and Holocene. The average LGM value of $\delta^{13}\text{CO}_2$ is
11 about -6.6‰ , which is only by 0.1‰ smaller than the Holocene value (-6.5‰). If
12 $\delta^{13}\text{CO}_2$ were influenced by changes in land carbon only, changes in $\delta^{13}\text{CO}_2$ should be
13 about $0.3\text{--}0.4\text{‰}$. This suggests that atmospheric $\delta^{13}\text{CO}_2$ is controlled not only by the
14 land carbon balance but also other factors such as changes in oceanic circulation and
15 marine biology [Brovkin *et al.*, 2002b]. In the G simulation with circulation changes
16 only, atmospheric $\delta^{13}\text{CO}_2$ was not affected at all (Table 3), despite a decrease in $\delta^{13}\text{C}$
17 in the deep Atlantic. This is caused by a redistribution of ocean ^{13}C , with an increase in the
18 surface Atlantic and Pacific (Fig. 6a). In the GN simulation, an enhanced biological
19 pump amplified the $\delta^{13}\text{C}$ gradient between deep and surface waters and led to an
20 increase of atmospheric $\delta^{13}\text{CO}_2$ by 0.3‰ . Land carbon release in the GNL simulation
21 draws $\delta^{13}\text{CO}_2$ down by 0.3‰ to a level of -6.6‰ , in line with ice core data. Other
22 factors, such as sea level change, did not significantly contribute.

23 Discussion

24 Coupled model simulations of the glacial climate published to date show no
25 consistency in changes of the Atlantic circulation. Some models show a pronounced
26 weakening and shoaling of the Atlantic meridional overturning circulation [e.g., Kim *et al.*
27 *et al.*, 2003; Shin *et al.*, 2003], and others show the opposite [e.g., Hewitt *et al.*, 2001;
28 Kitoh *et al.*, 2001]. The latest set of LGM experiments performed with several GCMs
29 and models of intermediate complexity, within the PMIP-2 project using identical
30 glacial boundary conditions, shows the same discrepancy between different models
31 (S.L. Weber, personal communication).

1 Results of the CLIMBER-2 model are most similar to simulations performed with the
2 CCSM climate model by *Shin et al.* [2003], who also found a shoaling and a weakening
3 of the Atlantic meridional circulation, a pronounced increase of salinity and an
4 intensification of AABW formation. This type of glacial ocean circulation changes is
5 supported by proxy data for Atlantic meridional overturning [*McManus et al.*, 2004],
6 and a dominance of low ^{13}C and ^{14}C Antarctic water in the glacial Atlantic ocean below
7 2-2.5 km depth [*Duplessy et al.*, 1988; *Curry and Oppo*, 2005; *Robinson et al.*, 2005].

8 These changes in AABW, and the associated increase in DIC in the deep North
9 Atlantic, explain about 40 ppm of the glacial pCO_2 drawdown. An additional 40ppm
10 decrease in pCO_2 is a consequence of increased nutrient utilization in the in Atlantic and
11 Indian sectors of the sub-Antarctic, as reconstructed from proxy data [*Kohfeld et al.*,
12 2005]. Although the total ocean productivity is enhanced by only 20%, the proximity to
13 the AABW formation region increases the sensitivity of atmospheric pCO_2 to the
14 biological pump here [*Marinov et al.*, 2006]. Without increased nutrient utilization, we
15 are not able to explain the absence of a glacial to interglacial $\delta^{13}\text{CO}_2$ change recorded in
16 the ice cores [*Smith et al.*, 1999].

17 In total, all five mechanisms represented in the G to GNLSC simulations, which we
18 rate to be of high and medium confidence (Table 3), are together able to explain a 65
19 ppm drop in pCO_2 , as compared to 80-90 ppm recorded in the ice cores. The shortfall
20 could be due to other, less well-documented mechanisms, or possibly due a quantitative
21 underestimation of the mechanisms as captured in our model. For example, the
22 simulated global LGM cooling in this series of experiments is 5 °C and thus in the lower
23 part of the best estimate range of 5.8 ± 1.4 °C found by *Schneider von Deimling et al.*
24 [2006a] by constraining a large model ensemble with proxy data. A greater cooling
25 would have enhanced several of the mechanisms considered here.

26 CO_2 changes from the different mechanisms probably follow a distinct sequence
27 around the glacial cycle. The CO_2 drawdown based on physical changes in ocean
28 circulation is probably most important in the early stages of glaciation. An ice sheet
29 nucleates in response to insolation changes towards the end of an interglacial climate
30 state, with interglacial pCO_2 levels. The ice sheet modifies the climate of the North
31 Atlantic, but would initially have had minor climate impacts elsewhere. Both cooling
32 and retention of freshwater in the ice sheet would make NADW denser. The cooling of

1 North Atlantic would lead to initial CO₂ drawdown, an increase of the southern
2 hemisphere sea ice cover, and consequent intensification of AABW which gradually
3 getting dense and starts to replace NADW in the abyssal Atlantic. These circulation
4 changes would result in cooling of the deep ocean and additional lowering of the
5 atmospheric CO₂. Fertilization of the sub-Antarctic ocean probably kicks in only later
6 during a glacial stage. Dust fluxes in Antarctica only increase from interglacial values
7 when the δ¹⁸O is at its negative extreme, in the coldest of the cold climates [Ridgwell,
8 2003].

9

10 **References**

- 11 Adkins, J. F., K. McIntyre, and D. P. Schrag (2002), The salinity, temperature, and delta
12 O-18 of the glacial deep ocean, *Science*, 298, 1769-1773.
- 13 Archer, D. (1996), A data-driven model of the global calcite lysocline, *Global*
14 *Biogeochemical Cycles*, 10, 511-526.
- 15 Archer, D., P. Martin, B. Buffett, V. Brovkin, S. Rahmstorf, and A. Ganopolski (2004),
16 The importance of ocean temperature to global biogeochemistry, *Earth and*
17 *Planetary Science Letters*, 222, 333-348.
- 18 Archer, D., A. Winguth, D. Lea, and N. Mahowald (2000), What caused the
19 glacial/interglacial atmospheric pCO₂ cycles?, *Reviews of Geophysics*, 38, 159-189.
- 20 Archer, D. E. (1991), Modeling the calcite lysocline, *J. Geophys. Res.*, 96, 17,037-
21 017,050.
- 22 Archer, D. E., and E. Maier-Reimer (1994), Effect of deep-sea sedimentary calcite
23 preservation on atmospheric CO₂ concentration, *Nature*, 367, 260-264.
- 24 Berger, A. L. (1978), Long-term variations of daily insolation and quaternary climatic
25 changes, *J. Atmospheric Sci.*, 35, 2362-2368.
- 26 Bopp, L., K. E. Kohfeld, C. Le Quere, and O. Aumont (2003), Dust impact on marine
27 biota and atmospheric CO₂ during glacial periods, *Paleoceanography*, 18.
- 28 Broecker, W. S., and T. H. Peng (1982), *Tracers in the sea*, Lamont-Doherty Geological
29 Observatory of Columbia University, Palisades, New York.
- 30 Brovkin, V., J. Bendtsen, M. Claussen, A. Ganopolski, C. Kubatzki, V. Petoukhov, and
31 A. Andreev (2002a), Carbon cycle, vegetation, and climate dynamics in the
32 Holocene: Experiments with the CLIMBER-2 model, *Global Biogeochemical*
33 *Cycles*, 16, doi:10.1029/2001GB001662.
- 34 Brovkin, V., M. Hofmann, J. Bendtsen, and A. Ganopolski (2002b), Ocean biology
35 could control atmospheric delta C-13 during glacial-interglacial cycle, *Geochemistry*
36 *Geophysics Geosystems*, 3, doi:10.1029/2001GC000270.
- 37 Catubig, N., D. E. Archer, R. Francois, P. deMenocal, and W. Howard (1998), Global
38 deep-sea burial rate of calcium carbonate during the Last Glacial Maximum,
39 *Paleoceanography*, 13, 298-310.
- 40 Crowley, T. J. (1995), Ice-Age Terrestrial Carbon Changes Revisited, *Global*
41 *Biogeochemical Cycles*, 9, 377-389.

- 1 Curry, W. B., and D. W. Oppo (2005), Glacial water mass geometry and the distribution
2 of delta C-13 of Sigma CO2 in the western Atlantic Ocean, *Paleoceanography*, 20,
3 doi:10.1029/2004PA001021.
- 4 Duplessy, J. C., N. J. Shackleton, R. G. Fairbanks, L. Labeyrie, and D. Oppo (1988),
5 Deep water source variations during the last climatic cycle and their impact on the
6 global deep water circulation, *Paleoceanography*, 3, 343-360.
- 7 Francois, L. M., Y. Godderis, P. Warnant, G. Ramstein, N. de Noblet, and S. Lorenz
8 (1999), Carbon stocks and isotopic budgets of the terrestrial biosphere at mid-
9 Holocene and last glacial maximum times, *Chemical Geology*, 159, 163-189.
- 10 Ganopolski, A., V. Petoukhov, S. Rahmstorf, V. Brovkin, M. Claussen, A. Eliseev, and
11 C. Kubatzki (2001), CLIMBER-2: a climate system model of intermediate
12 complexity. Part II: model sensitivity, *Climate Dynamics*, 17, 735-751.
- 13 Harrison, S. P., and A. I. Prentice (2003), Climate and CO2 controls on global
14 vegetation distribution at the last glacial maximum: analysis based on
15 palaeovegetation data, biome modelling and palaeoclimate simulations, *Global
16 Change Biology*, 9, 983-1004.
- 17 Hewitt, C. D., A. J. Broccoli, J. F. B. Mitchell, and R. J. Stouffer (2001), A coupled
18 model study of the last glacial maximum: Was part of the North Atlantic relatively
19 warm?, *Geophysical Research Letters*, 28, 1571-1574.
- 20 Jahn, A., M. Claussen, A. Ganopolski, and V. Brovkin (2005), Quantifying the effect of
21 vegetation dynamics on the climate of the Last Glacial Maximum, *Climate of the
22 Past*, 1, 1-7, www.climate-of-the-past.net/cp/1/1/.
- 23 Joos, F., S. Gerber, I. C. Prentice, B. L. Otto-Bliesner, and P. J. Valdes (2004),
24 Transient simulations of Holocene atmospheric carbon dioxide and terrestrial carbon
25 since the Last Glacial Maximum, *Global Biogeochemical Cycles*, 18.
- 26 Kim, S. J., G. M. Flato, and G. J. Boer (2003), A coupled climate model simulation of
27 the last glacial maximum, Part 2: approach to equilibrium, *Climate Dynamics*, 20,
28 635-661.
- 29 Kitoh, A., S. Murakami, and H. Koide (2001), A simulation of the last glacial maximum
30 with a coupled atmosphere-ocean GCM, *Geophysical Research Letters*, 28, 2221-
31 2224.
- 32 Kleypas, J. A. (1997), Modeled estimates of global reef habitat and carbonate
33 production since the last glacial maximum, *Paleoceanography*, 12, 533-545.
- 34 Kohfeld, K. E., C. Le Quere, S. P. Harrison, and R. F. Anderson (2005), Role of marine
35 biology in glacial-interglacial CO2 cycles, *Science*, 308, 74-78.
- 36 Kohler, P., H. Fischer, G. Munhoven, and R. E. Zeebe (2005), Quantitative
37 interpretation of atmospheric carbon records over the last glacial termination, *Global
38 Biogeochemical Cycles*, 19.
- 39 Mahowald, N., K. Kohfeld, M. Hansson, Y. Balkanski, S. P. Harrison, I. C. Prentice, M.
40 Schulz, and H. Rodhe (1999), Dust sources and deposition during the last glacial
41 maximum and current climate: A comparison of model results with paleodata from
42 ice cores and marine sediments, *Journal of Geophysical Research-Atmospheres*, 104,
43 15895-15916.
- 44 Marinov, I., A. Gnanadesikan, J. R. Toggweiler, and J. L. Sarmiento (2006), The
45 Southern Ocean biogeochemical divide, *Nature*, 441, 964-967.
- 46 Martin, P., D. Archer, and D. Lea (2002), The role of deep sea temperature change in
47 the glacial carbon cycle, *Geochimica Et Cosmochimica Acta*, 66, A488-A488.
- 48 Martin, P., D. Archer, and D. Lea (2005), Role of deep sea temperatures in the carbon
49 cycle during the last glacial, *Paleoceanography*, doi:10.1029/2003PA000914.

- 1 Matsumoto, K., J. L. Sarmiento, and M. A. Brzezinski (2002), Silicic acid "leakage"
2 from the Southern Ocean as a possible mechanism for explaining glacial atmospheric
3 pCO₂, *Global Biogeochemical Cycles*, 16, 10.1029/2001GB001442.
- 4 McManus, J. F., R. Francois, J. M. Gherardi, L. D. Keigwin, and S. Brown-Leger
5 (2004), Collapse and rapid resumption of Atlantic meridional circulation linked to
6 deglacial climate changes, *Nature*, 428, 834-837.
- 7 Munhoven, G. (2002), Glacial-interglacial changes of continental weathering: estimates
8 of the related CO₂ and HCO₃⁻ flux variations and their uncertainties, *Global and
9 Planetary Change*, 33, 155-176.
- 10 Peltier, W. R. (1994), Ice-Age Paleotopography, *Science*, 265, 195-201.
- 11 Petit, J. R., J. Jouzel, D. Raynaud, N. I. Barkov, J. M. Barnola, I. Basile, M. Bender, J.
12 Chappellaz, M. Davis, G. Delaygue, M. Delmotte, V. M. Kotlyakov, M. Legrand, V.
13 Y. Lipenkov, C. Lorius, L. Pepin, C. Ritz, E. Saltzman, and M. Stievenard (1999),
14 Climate and atmospheric history of the past 420,000 years from the Vostok ice core,
15 Antarctica, *Nature*, 399, 429-436.
- 16 Petoukhov, V., A. Ganopolski, V. Brovkin, M. Claussen, A. Eliseev, C. Kubatzki, and
17 S. Rahmstorf (2000), CLIMBER-2: a climate system model of intermediate
18 complexity. Part I: model description and performance for present climate, *Climate
19 Dynamics*, 16, 1-17.
- 20 Prentice, I. C., and D. Jolly (2000), Mid-Holocene and glacial-maximum vegetation
21 geography of the northern continents and Africa, *Journal of Biogeography*, 27, 507-
22 519.
- 23 Rea, D. K. (1994), The paleoclimatic record provided by eolian deposition in the deep
24 sea: The geologic history of wind, *Reviews of Geophysics*, 32, 159-196.
- 25 Ridgwell, A. J. (2003), Implications of the glacial CO₂ "iron hypothesis" for Quaternary
26 climate change, *Geochemistry Geophysics Geosystems*, 4.
- 27 Robinson, L. F., J. F. Adkins, L. D. Keigwin, J. Southon, D. P. Fernandez, S. L. Wang,
28 and D. S. Scheirer (2005), Radiocarbon variability in the western North Atlantic
29 during the last deglaciation, *Science*, 310, 1469-1473.
- 30 Scheffer, M., V. Brovkin, and P. M. Cox (2006), Positive feedback between global
31 warming and atmospheric CO₂ concentration inferred from past climate change,
32 *Geophysical Research Letters*, 33, doi:10.1029/2005GL025044.
- 33 Schmittner, A. (2003), Southern Ocean sea ice and radiocarbon ages of glacial bottom
34 waters, *Earth and Planetary Science Letters*, 213, 53-62.
- 35 Schneider von Deimling, T., A. Ganopolski, H. Held, and S. Rahmstorf (2006a), How
36 cold was the Last Glacial Maximum?, *Geophysical Research Letters*, 33.
- 37 Schneider von Deimling, T., H. Held, A. Ganopolski, and S. Rahmstorf (2006b),
38 Climate sensitivity estimated from ensemble simulations of glacial climate, *Climate
39 Dynamics*, 27, 149-163.
- 40 Shackleton, N. J. (1977), Carbon 13 in *Uvigerina*: tropical rainforest history and the
41 equatorial Pacific carbonate dissolution cycles. in *The Fate of Fossil Fuel CO₂ in the
42 Oceans*, edited by Andersen, N. R. and A. Malahoff, pp. 401-428, Plenum Press,
43 New York.
- 44 Shin, S. I., Z. Liu, B. Otto-Bliesner, E. C. Brady, J. E. Kutzbach, and S. P. Harrison
45 (2003), A simulation of the last glacial maximum climate using the NCAR-CCSM,
46 *Climate Dynamics*, 20, 127-151.
- 47 Siegenthaler, U., T. F. Stocker, E. Monnin, D. Luthi, J. Schwander, B. Stauffer, D.
48 Raynaud, J. M. Barnola, H. Fischer, V. Masson-Delmotte, and J. Jouzel (2005),
49 Stable carbon cycle-climate relationship during the late Pleistocene, *Science*, 310,
50 1313-1317.

1 Sigman, D. M., and E. A. Boyle (2000), Glacial/interglacial variations in atmospheric
2 carbon dioxide, *Nature*, 407, 859-869.

3 Smith, H. J., H. Fischer, M. Wahlen, D. Mastroianni, and B. Deck (1999), Dual modes
4 of the carbon cycle since the Last Glacial Maximum, *Nature*, 400, 248-250.

5 Toggweiler, J. R., J. L. Russell, and S. R. Carson (2006), Midlatitude westerlies,
6 atmospheric CO₂, and climate change during the ice ages, *Paleoceanography*, 21,
7 doi:10.1029/2005PA001154.

8 Torn, M. S., and J. Harte (2006), Missing feedbacks, asymmetric uncertainties, and the
9 underestimation of future warming, *Geophysical Research Letters*, 33,
10 doi:10.1029/2005GL025540.

11 Watson, A. J., and A. C. N. Garabato (2006), The role of Southern Ocean mixing and
12 upwelling in glacial-interglacial atmospheric CO₂ change, *Tellus Series B-Chemical
13 and Physical Meteorology*, 58, 73-87.

14

1 Table 1. Description of simulations

Simulation	Factor				
	Glacial circulation/ SST changes	Nutrient utilization in subantarctic Atlantic and Indian sectors	Land carbon reduction (540 GtC)	Sea level change (3% change in volume, ALK, PO ₄)	50%-reduction in shallow water sedimentation
CTRL	-	-	-	-	-
G	+	-	-	-	-
GN	+	+	-	-	-
GNL	+	+	+	-	-
GNLS	+	+	+	+	-
GNLSC	+	+	+	+	+

2

3

1 Table 2. Simulation results

Simulation	Atmospheric pCO ₂ , ppm	Export flux at sea surface, GtC/yr	CaCO ₃ flux at sea floor, GtC/yr	ALK _{ave} , μmol/kg	DIC _{ave} , μmol/kg	Atmospheric δ ¹³ CO ₂ , ‰
CTRL	280	7.7	0.40	2373	2233	-6.50
G (circulation and SST)	237	7.4	0.4	2410	2262	-6.48
GN (+ nutrients)	200	9.2	0.42	2437	2284	-6.20
GNL (+ land)	215	9.2	0.42	2502	2352	-6.61
GNLS (+ sea level)	227	9.3	0.42	2573	2423	-6.60
GNLSC (+ coral reefs)	215	9.3	0.42	2630	2459	-6.64

2

1 Table 3. Mechanism contributions to glacial pCO₂ changes

Mechanism	Simulated $\Delta p\text{CO}_2$ (ppm) after carbonate compensation	Confidence level	Proxy data in support of the model results
Circulation and SST	-43	High	Oceanic $\delta^{13}\text{C}$
Sea level	12	High	Oceanic $\delta^{18}\text{O}$
Nutrient utilization in subantartic, Atlantic & Indian ocean	-37	Medium	^{15}N , $\delta^{13}\text{Si}$
Land carbon	15	Medium	Pollen records, oceanic $\delta^{13}\text{C}$, atmospheric $\delta^{13}\text{C}$
Shallow water carbonate sedimentation	-12	Medium	Excessive corals accumulation in Holocene
Subtotal:	-65		
10% decrease in weathering	2	Low	
20% decrease in rain ratio	-15	Low	
Nutrients utilization in subantarctic Pacific	-7	Low	
Total:	-85		

2

1 **Figure captions**

2 Figure 1. Simulated circulation and salinity in Atlantic basin for present-day simulation
3 CTRL (A) and glacial simulation G (B). Left: overturning (Sv). Right: salinity (psu).

4
5 Figure 2. Glacial changes in oceanic: A) temperature (°C); B) DIC distribution
6 (μmol/kg). Shown is a difference between simulations G and CTRL.

7
8 Figure 3. Dynamics of atmospheric $p\text{CO}_2$ (ppm) in the G simulation. Initial conditions
9 were from the CTRL simulation. Imposed glacial boundary conditions are explained in
10 the text.

11
12 Figure 4. Glacial changes in oceanic DIC distribution (μmol/kg). A) simulation GN; B)
13 simulation GNLS; C) simulation GNLSC. Shown is a difference between the given
14 simulation and simulation CTRL.

15
16 Figure 5. CaCO_3 (%) in top layer of sediments. A) Observations [Archer, 1996]
17 averaged on the CLIMBER-2 grid with three basin and 10° latitudinal resolution; B)
18 simulation CTRL; C) simulation CNLS; D) simulation GNLSC.

19
20 Figure 6. Glacial changes in oceanic $\delta^{13}\text{C}$ distribution (‰). A) simulation G; B)
21 simulation GN; C) simulation GNLSC. Shown is a difference between the given
22 simulation and simulation CTRL.

23
24 Figure 7. Modern (top) and glacial (bottom) distribution of $\delta^{13}\text{C}$ in Atlantic (‰). Left,
25 figure from Duplessy *et al.* [1988] reproduced after Ruddiman [2001] (permission
26 required). Right, results from the CTRL (top) and GNLSC (bottom) simulations. The
27 color bar to the right is for the model results.

28
29
30

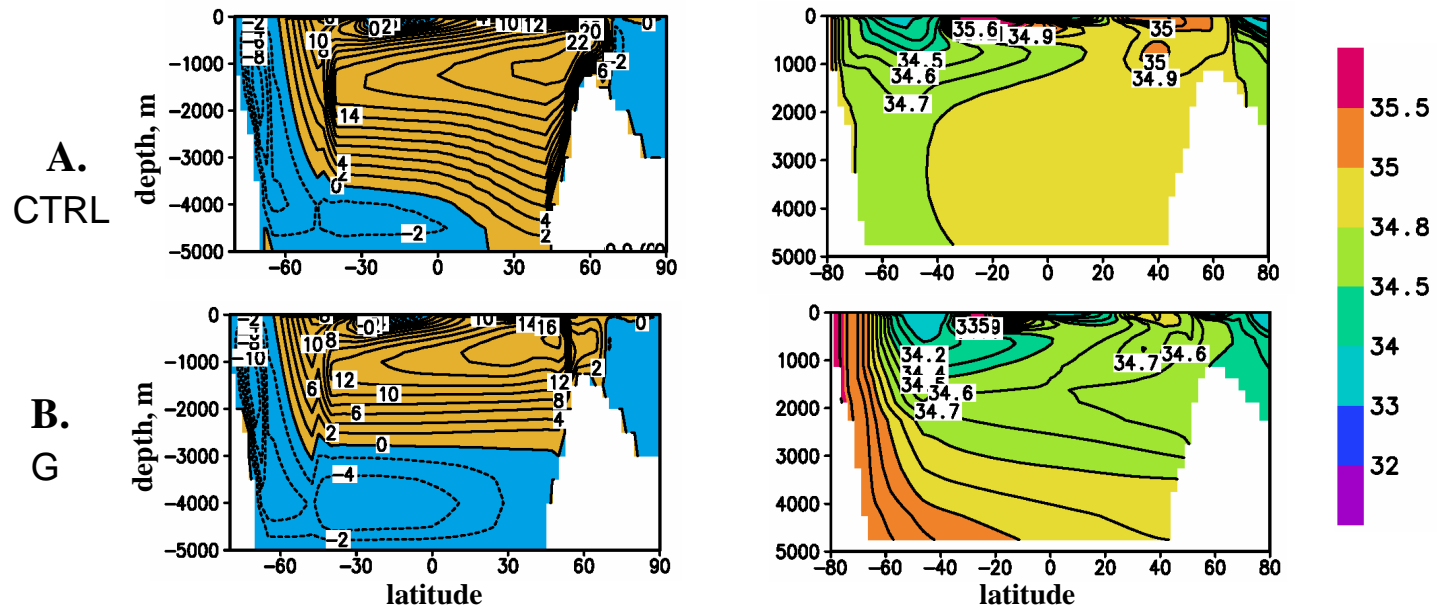


Figure 1

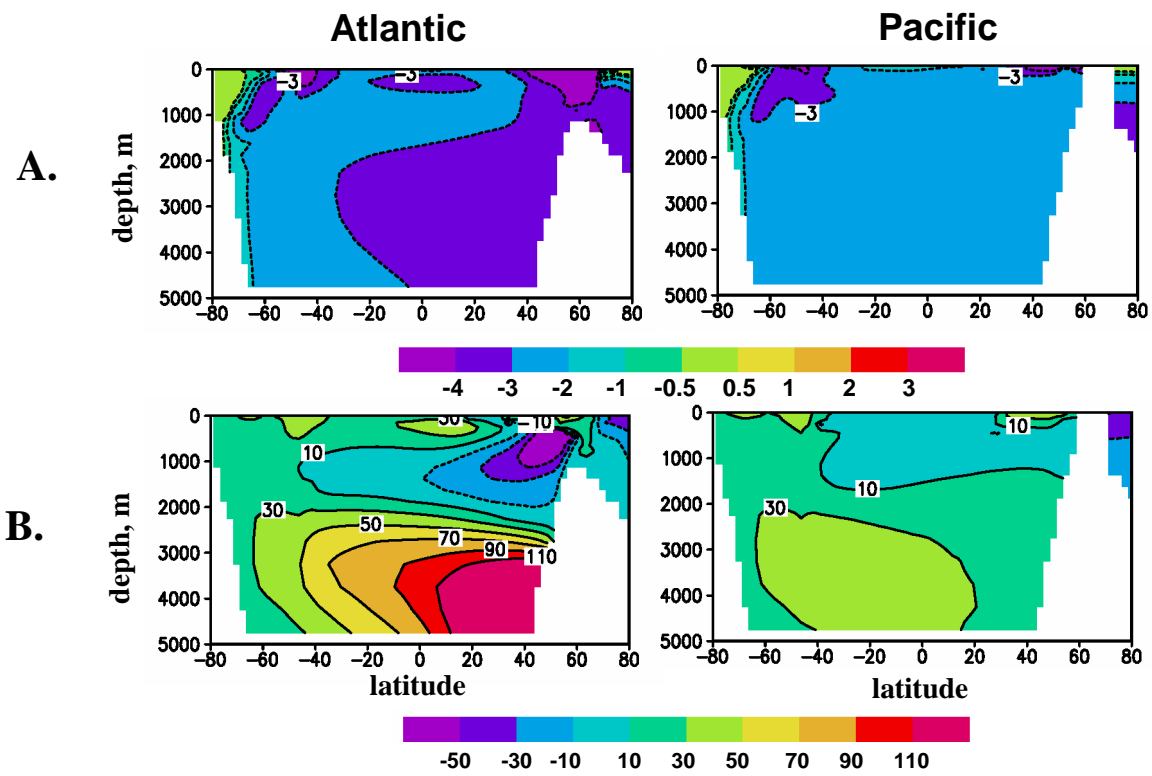


Figure 2

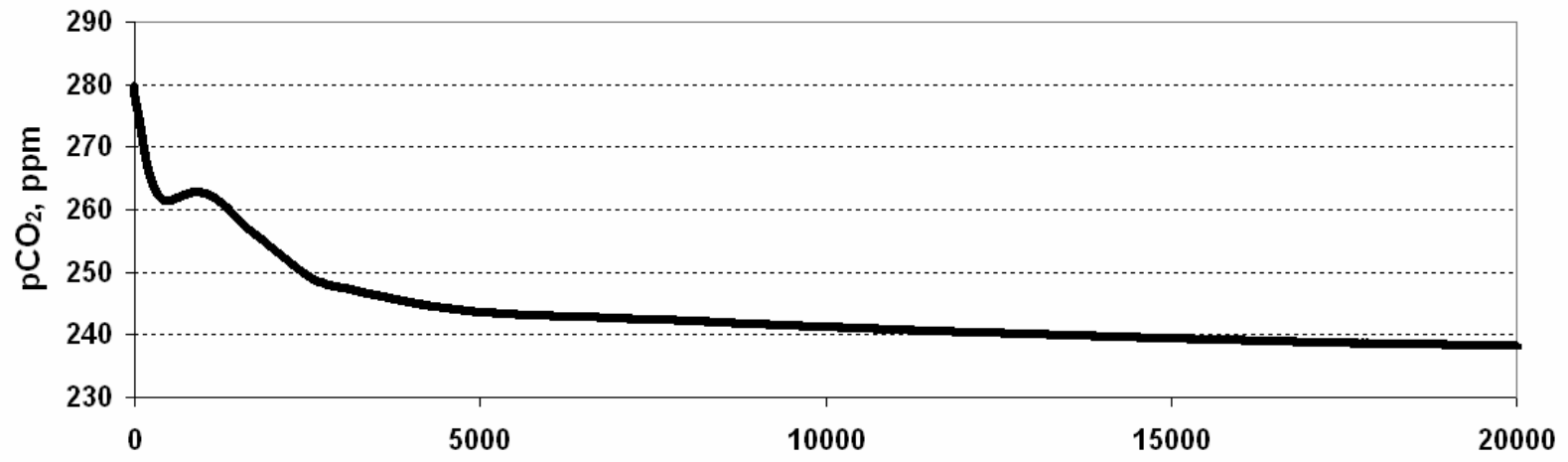


Figure 3

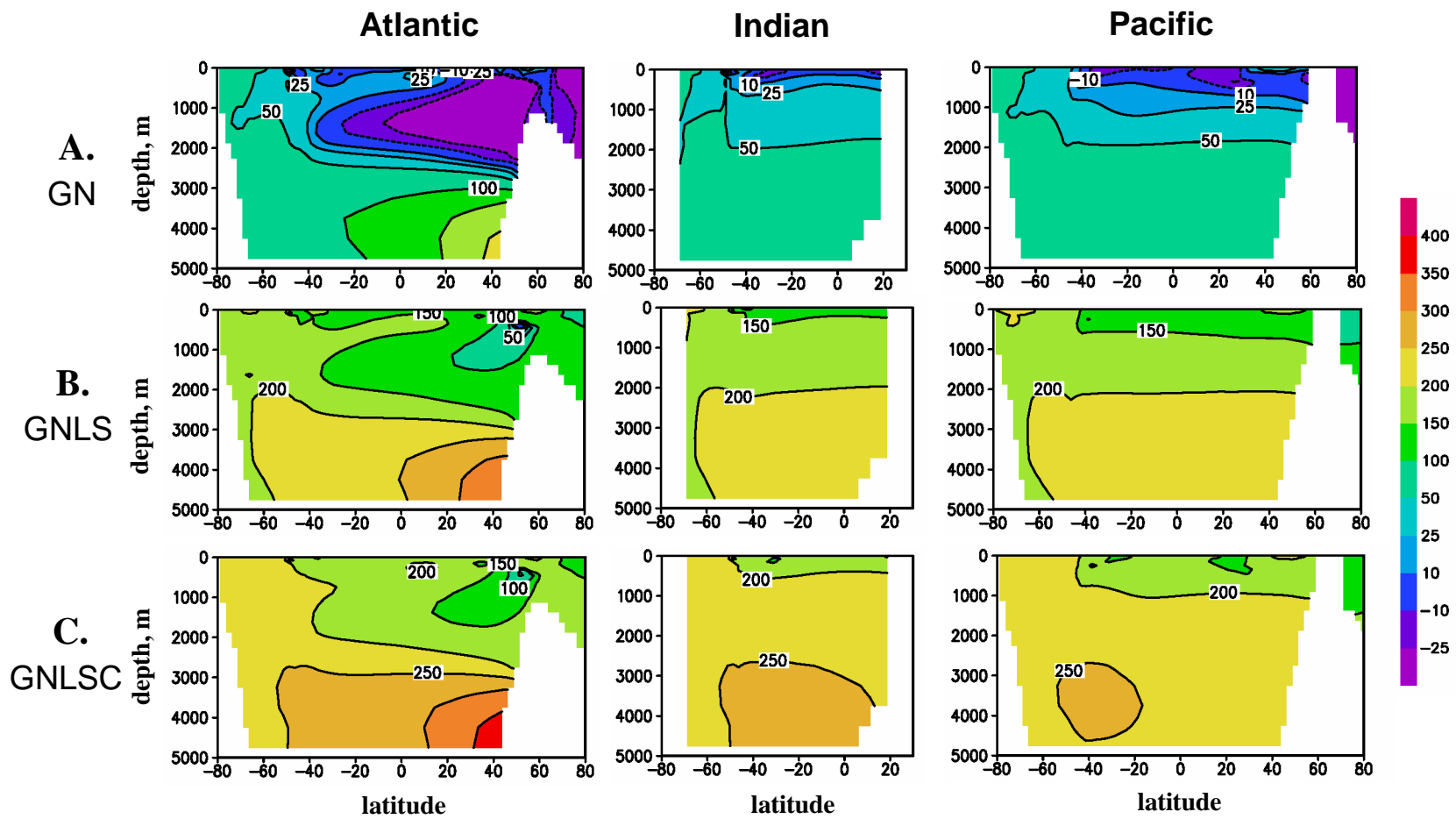


Figure 4

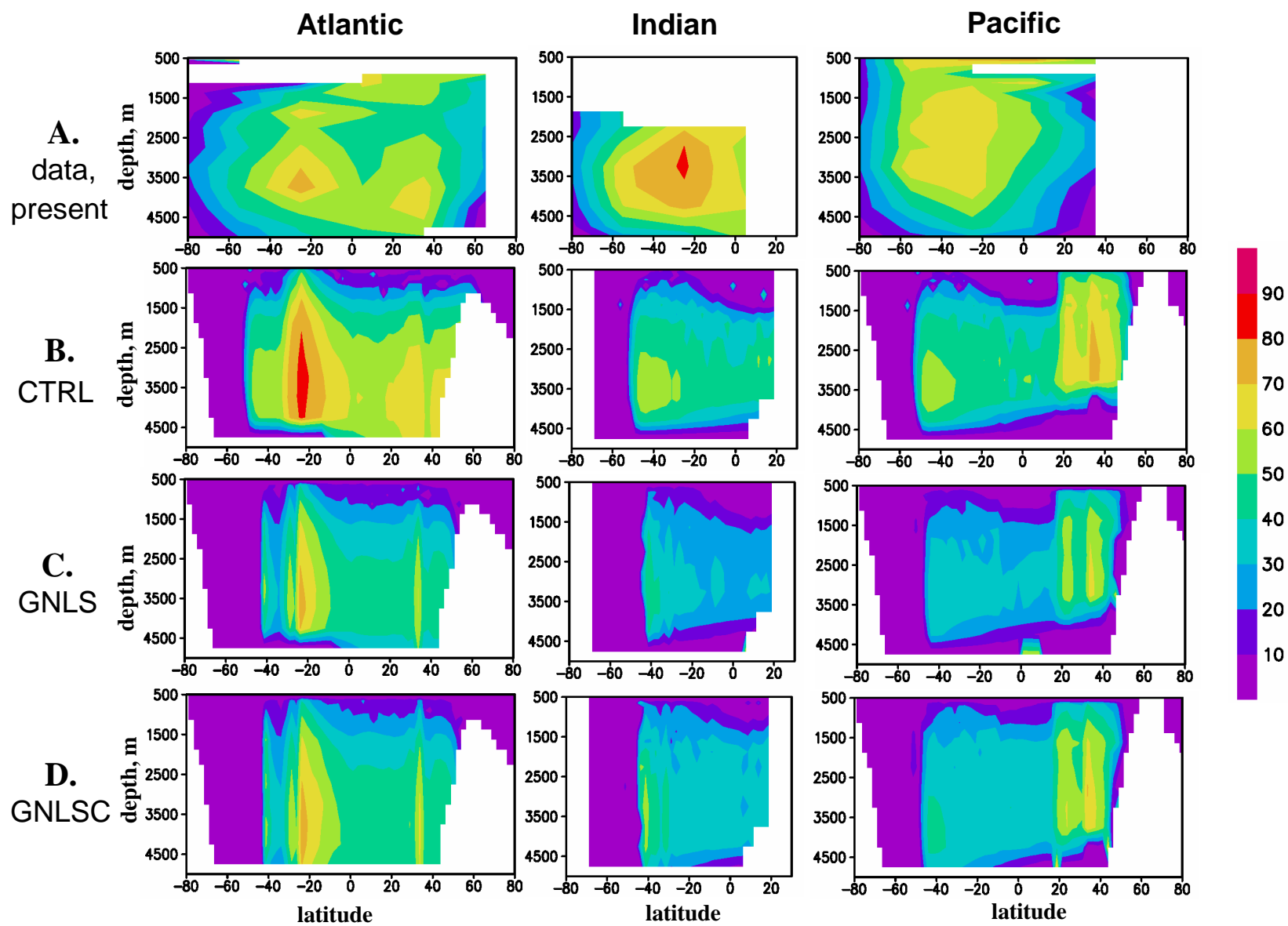


Figure 5

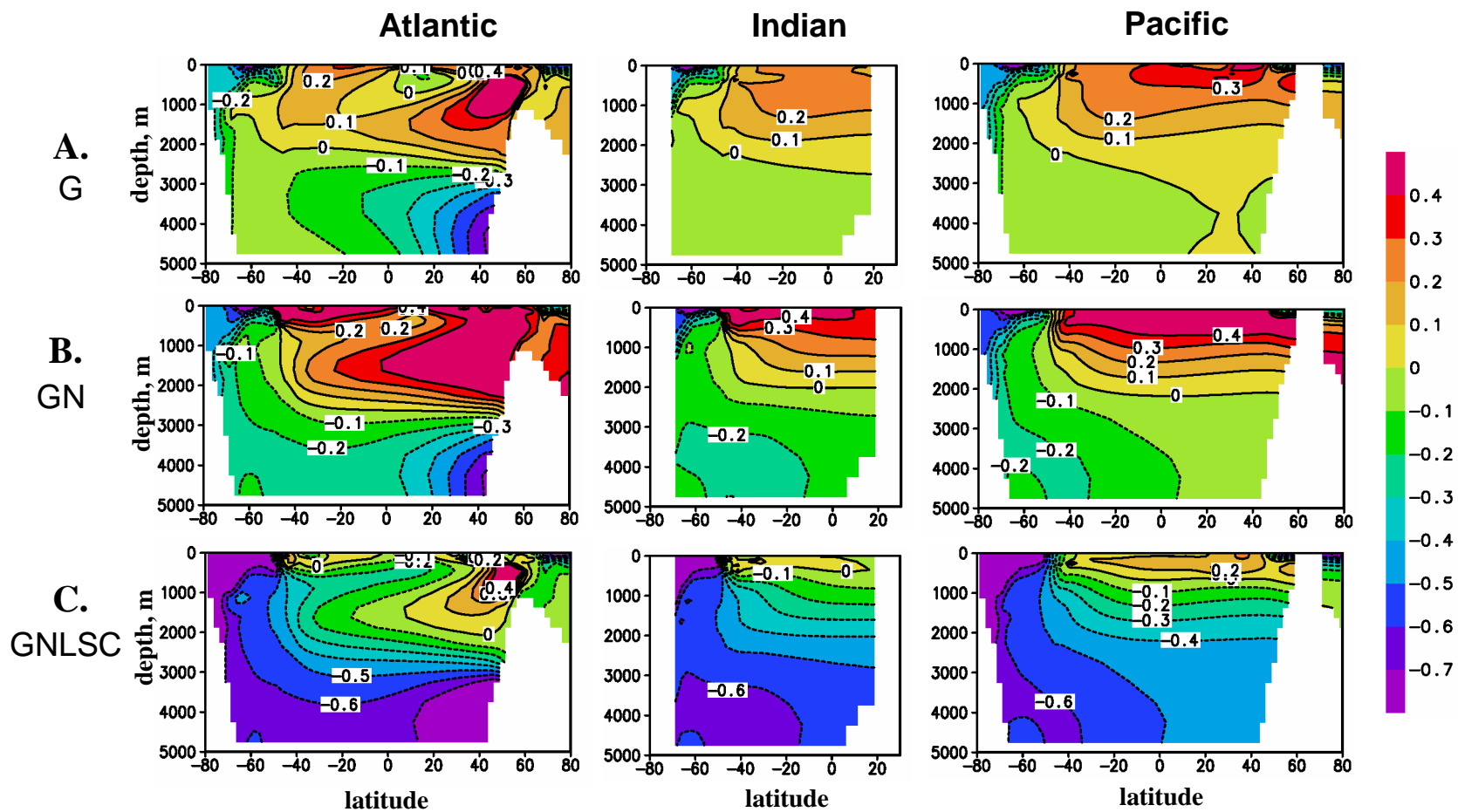


Figure 6

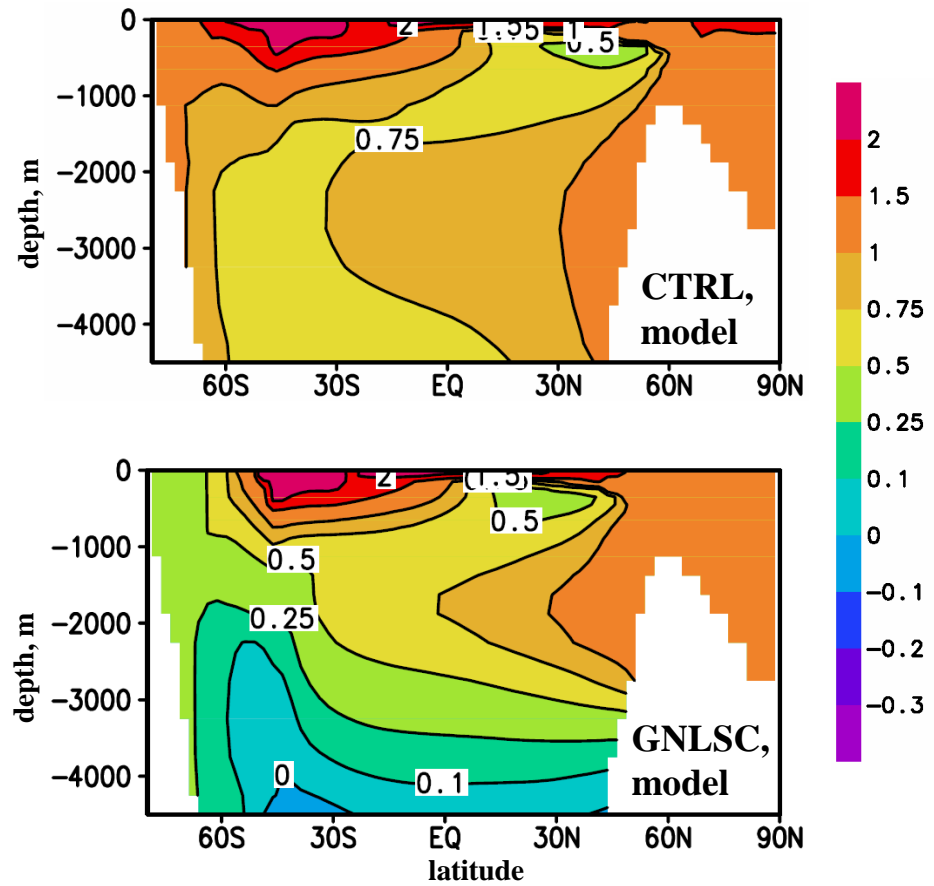
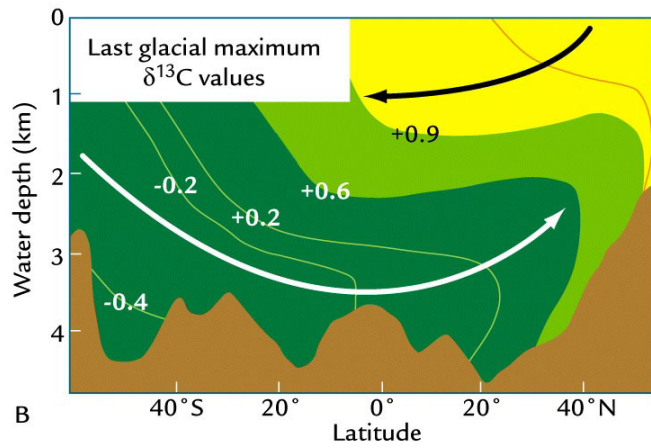
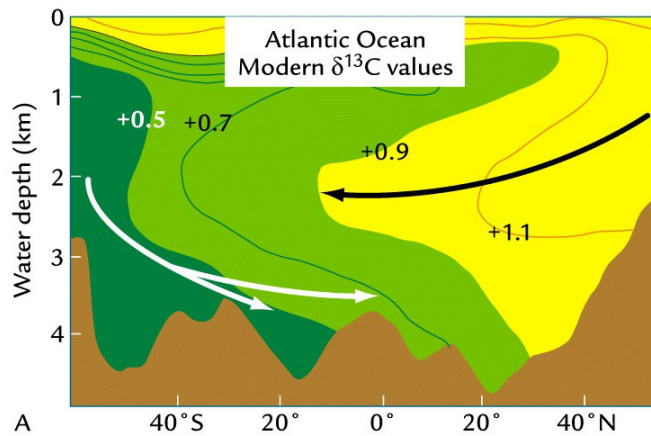


Figure 7